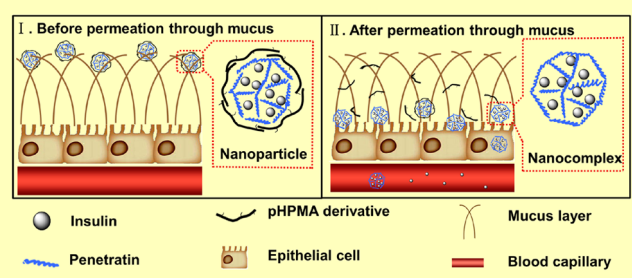


Overcoming the Diffusion Barrier of Mucus and Absorption Barrier of Epithelium by Self-Assembled Nanoparticles for Oral Delivery of Insulin

Wei Shan, Xi Zhu, Min Liu, Lian Li, Jiaju Zhong, Wei Sun, Zhirong Zhang, and Yuan Huang*

Key Laboratory of Drug Targeting and Drug Delivery System, Ministry of Education, West China School of Pharmacy, Sichuan University, No. 17, Block 3, Southern Renmin Road, Chengdu, Sichuan 610041, PR China

ABSTRACT Nanoparticles (NPs) have demonstrated great potential for the oral delivery of protein drugs that have very limited oral bioavailability. Orally administered NPs could be absorbed by the epithelial tissue only if they successfully permeate through the mucus that covers the epithelium. However, efficient epithelial absorption and mucus permeation require very different surface properties of a nanocarrier. We herein report self-assembled NPs for efficient oral delivery of insulin by facilitating both of these two processes. The NPs possess a nanocomplex core composed of insulin and cell penetrating peptide (CPP), and a dissociable hydrophilic coating of *N*-(2-hydroxypropyl) methacrylamide copolymer (pHPMA) derivatives. After systematic screening using mucus-secreting epithelial cells, NPs exhibit excellent permeation in mucus due to the “mucus-inert” pHPMA coating, as well as high epithelial absorption mediated by CPP. The investigation of NP behavior shows that the pHPMA molecules gradually dissociate from the NP surface as it permeates through mucus, and the CPP-rich core is revealed in time for subsequent transepithelial transport through the secretory endoplasmic reticulum/Golgi pathway and endocytic recycling pathway. The NPs exhibit 20-fold higher absorption than free insulin on mucus-secreting epithelium cells, and orally administered NPs generate a prominent hypoglycemic response and an increase of the serum insulin concentration in diabetic rats. Our study provides the evidence of using pHPMA as dissociable “mucus-inert” agent to enhance mucus permeation of NPs, and validates a strategy to overcome the multiple absorption barriers using NP platform with dissociable hydrophilic coating and drug-loaded CPP-rich core.



KEYWORDS: oral delivery · insulin · nanoparticles · mucus · epithelium · cell penetrating peptide

Protein therapeutics are increasingly being applied for the treatment of various diseases in clinic due to their high therapeutic efficacy and excellent selectivity.¹ Despite the frequent dosing that is required for patients with many diseases, especially chronic ones, the administration of these drugs are largely limited to parenteral routes and, thus, causes problems including low patient compliance and safety issues.² The oral bioavailability of these biomolecules is very limited (<1%) due to their inherent low permeability across the epithelium and the rapid digestive degradation.³ The advance of nanotechnology and nanomedicine in the past decade has opened a new perspective for oral delivery of biomolecules. Numerous

nanocarriers have been reported for the oral delivery application, such as liposomes, nanogels, and polymeric nanoparticles (NPs).^{4,5} Improved bioavailability was achieved with these nanocarriers utilizing different absorption strategies, such as paracellular permeation through opened tight junctions and transcytosis mediated by certain receptors.^{6,7}

Different from the NPs developed for parenteral application, the behavior of orally administered NPs is greatly influenced by their interaction with the mucus that covers and protects the underlying epithelium.⁸ Intestinal mucus is a layer of slippery secretion in constant and fast renewal and, thus, can rapidly trap and remove foreign particles, especially those

* Address correspondence to
huangyuan0@163.com.

Received for review January 3, 2015
and accepted February 6, 2015.

Published online February 06, 2015
10.1021/acsnano.5b00028

© 2015 American Chemical Society

possessing cationic and hydrophobic nature in surface property.^{9,10} Reduced absorption of NPs caused by the mucus barrier has recently been paid increasing attention, and different techniques have been proposed to solve this problem.^{8,10–13} One excellent example is the development of Mucus Penetrating Particles (MPP) inspired by the virus that can freely diffuse through mucus.⁸ It was found that NPs with a densely PEGylated surface exhibited excellent diffusion ability in mucus. The hydrophilic and electrically neutral surface of the NP serves as “mucus-inert” interface that prevents the trapping of the particles, and facilitates their diffusion through the low viscosity pores in mucus matrix.¹⁰ However, it should be noted that mucus permeation and epithelial absorption require very different surface properties of a nanocarrier. As reported by different researchers, the hydrophilic and electro-neutral surface may prevent the interaction of NPs with the target cell membrane and, thus, may decrease their uptake by epithelial cells.^{14–16} Therefore, a nanocarrier designed for oral delivery should have the ability to conquer the obstacles of both mucus layer and epithelium.

Cell-penetrating peptides (CPPs) are short peptides that can facilitate cellular internalization of various molecular cargos.¹⁷ CPPs were also demonstrated to improve the transepithelial transport of different proteins in the forms of covalent conjugation¹⁵ or physical mixture.¹⁸ Previous study of our group demonstrated that nanocomplex (NC) prepared with penetratin (CRQIKIWFQNRRMKWKK), one of the most promising CPPs, effectively transported encapsulated insulin across epithelium.¹⁹ However, the cationic property of CPPs, which plays a vital role in their cellular internalization,²⁰ also induced a high affinity of CPP-rich particles with the negatively charged mucin that formed the mucus matrix and, thus, reduced their absorption efficiency.

We herein developed a self-assembled NP for oral delivery of protein drug, which was designed with a novel strategy to achieve both excellent mucus permeation and transepithelial absorption. With insulin as a model drug, the NPs possessed a CPP/protein nanocomplex core and an *N*-(2-hydroxypropyl) methacrylamide (HPMA) polymer (pHPMA) derivatives coating. HPMA polymer has been explored as a hydrophilic macromolecular carrier for chemotherapeutic agents for decades,^{21–24} and at least six HPMA-based therapeutics have currently progressed into phase I or phase II clinical trials.^{25,26} In our study, HPMA copolymer was validated for the first time as a dissociable “mucus-inert” coating material, which assembled on the NP surface to facilitate mucus permeation, while separated in time for subsequent CPP-mediated transport through epithelium. With the screening of pHPMAs with different charge density, and the investigation of the NP behavior in mucus and on the mucus-secreting epithelial cell, we demonstrated that the NP with CPP-rich core and

dissociable pHPMA coating could successfully solve the dilemma of choosing between high mucus permeation and high epithelial transport.

RESULTS

HPMA Polymer Synthesis. Different from other commonly used hydrophilic polymers (*e.g.*, PEG), the physiochemical properties of pHPMA can be easily tuned by manipulating the monomers. pHPMA derivatives were synthesized using radical solution polymerization method with negatively charged *N*-methacryloyl-glycylglycine (MA-GG-OH) monomer. The MA-GG-OH monomer was fed at three different ratios (5%, 10%, and 20%) in order to endow the pHPMA with different densities of negative charge, and the polymers were termed as pHPMA-1, pHPMA-2, and pHPMA-3, respectively (Figure 1A). The ¹H nuclear magnetic resonance (¹H NMR) spectra and mass spectrograms were recorded (Supporting Information Figures S1–S5). The molecular weight of the all pHPMA derivatives was ~45 kDa with a PDI less than 1.8 (Supporting Information Table S1). The charge density of three polymers was measured using titration method and was determined to be 0.28, 0.43, and 1.05 mmol/g, respectively (Figure 1B).

Preparation and Characterization of Nanoparticles. The nanoparticles are prepared through a two-step approach based on self-assembly strategy. Penetratin is a polycationic peptide that possesses strong affinity with negatively charged proteins.¹⁹ Aqueous solution of insulin and penetratin were first mixed at a weight ratio of 2:1 to form polyelectrolyte nanocomplexes (NCs). Then, by adding the NCs into a pHPMA solution, the positively charged NC and negatively charged pHPMA were spontaneously assembled to form NPs with nanocomplex core surrounded by pHPMA coating, as shown schematically in Figure 1C. NPs prepared with three pHPMAs were termed accordingly as NPs-1, NPs-2, and NPs-3, and another batch of NPs (NPs-4) was prepared with a higher amount of pHPMAs-3 in formulation (Table 1). The TEM images of NCs and NPs were shown in Figure 1D. The NCs exhibited a size of 148 nm as tested by dynamic light scattering, while the size of all pHPMA coated NPs was approximately 175 nm (Figure 1E). NPs in mucus were reported to transport primarily through lower viscosity pores within the elastic matrix, and the mesh spacing ranges approximately from 10 to 200 nm.¹⁰ Therefore, the NPs that were sub-200 nm in diameter could meet the sterical requirement for rapid diffusion. In addition, all NP exhibited insulin encapsulation efficiency above 80% and drug loading efficiency above 40%. The encapsulated insulin was released in a sustained manner within 10 h in phosphate buffered saline (pH 7.4) (Supporting Information Figure S6).

As shown in Figure 1E, the CPP-rich NCs were highly positively charged with zeta potential of 20.9 mV.

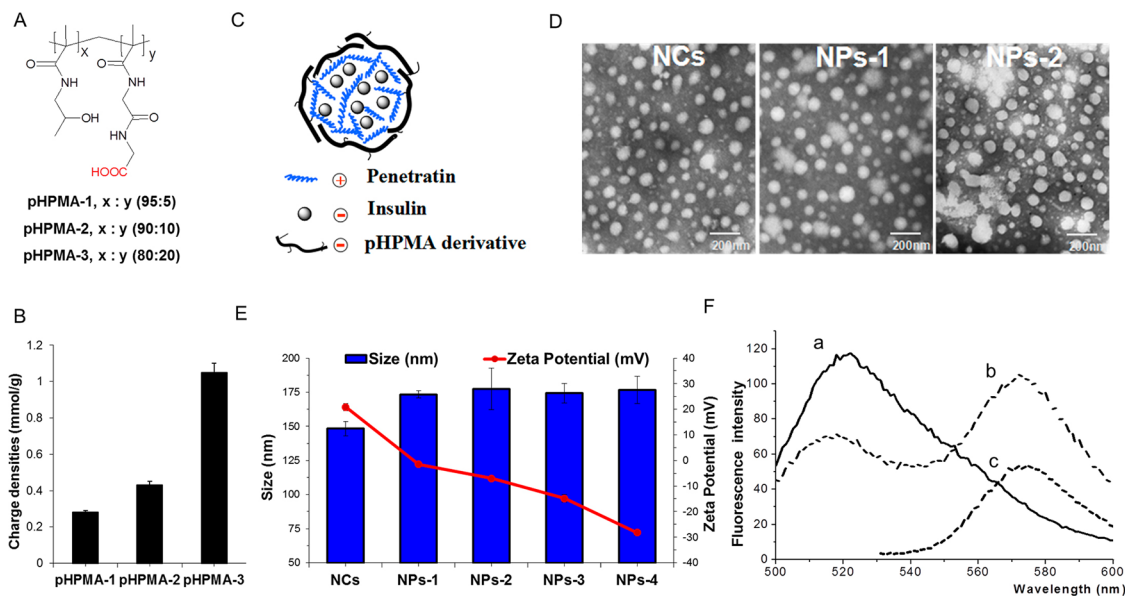


Figure 1. (A) Chemical structure of HPMA polymer derivatives with different ratio of MA-GG-OH monomer. (B) Charge densities of the three pHPMAs as measured by titration method. Data are means \pm SD ($n = 3$). (C) Schematic diagram of NP, which possessed a penetratin/insulin nanocomplex core with sheddable pHPMA coating. (D) TEM images of NCs, NPs-1 and NPs-2. (E) Size and zeta potential of NCs and different NPs. Data are means \pm SD ($n = 3$). (F) Emission spectrum of free F-insulin (a), NPs (b), and T-pHPMA (c) with excitation at 440 nm.

TABLE 1. Characterizations of NCs and NPs^a

sample	pHPMA	concentration mg/mL	size (nm)	PDI	EE (%)	DL (%)
NCs	-	-	148.3 \pm 5.1	0.31 \pm 0.09	95.3 \pm 1.6	65.6 \pm 4.0
NPs-1	pHPMA-1	2	173.4 \pm 2.7	0.22 \pm 0.02	94.4 \pm 1.7	48.5 \pm 6.7
NPs-2	pHPMA-2	1	177.3 \pm 15.2	0.24 \pm 0.03	94.9 \pm 1.1	52.6 \pm 1.5
NPs-3	pHPMA-3	1	174.4 \pm 7.2	0.26 \pm 0.03	89.1 \pm 3.5	49.9 \pm 7.6
NPs-4	pHPMA-3	2	176.7 \pm 9.8	0.24 \pm 0.02	83.8 \pm 4.4	44.4 \pm 5.6

^a Data are means \pm SD ($n = 3$).

After the pHPMA coating, the all NPs possessed a negative zeta potential ranging from -1.47 to -28.2 mV. Lower surface charge was observed with NPs prepared with pHPMA of higher charge density (NPs-2 and NPs-3) or with higher amount of pHPMA in the formulation (NPs-4). The reversal of surface charge suggested the successful coating of anionic pHPMA on the outer surface of the NPs. The coating of pHPMA was further validated using a fluorescence resonance energy transfer (FRET) analysis.²⁷ The NPs were prepared with TRITC labeled HPMA polymers (T-pHPMA) and FITC labeled insulin (F-insulin), which formed a FRET pair. The emission intensity of F-insulin decreased at 520 nm and that of TRITC increased at 573 nm, which implied the energy transfer from donor to acceptor (Figure 1F). The FRET efficiency between two interacting partners was 38.8% and the FRET distance was calculated to be 5.7 nm, which again suggested the formation of pHPMA coated NPs. Moreover, the enzymatic stability of the insulin encapsulated in the particles was investigated using trypsin and α -chymotrypsin. All NPs exhibited better protection for loaded insulin against digestive enzyme

compared with NCs or free insulin (Supporting Information Figures S7 and S8).

Mucus Permeation Ability of NPs. The mucus layer has evolved to protect the body with excellent ability to immobilize and remove cationic and hydrophobic molecules and particles.^{10,28} The negative charges of carboxyl or sulfate groups on the mucin proteoglycans and the periodic hydrophobic globular regions along mucin strands allow efficient formation of multiple low-affinity adhesive interactions with the cationic and hydrophobic regions on the surfaces of foreign substances.¹⁰ Since major types of proteins have both hydrophilic and hydrophobic region in their structures, and CPPs also possess strong polycationic character, the CPP–protein complex would exhibit high affinity with the mucin. We hypothesize that by concealing the nanocomplex beneath the negatively charged hydrophilic HPMA polymer, the particle could exhibit reduced interaction with the mucus layer. To test our hypothesis, we first evaluated the interaction of the particles with mucin by measuring the amount of particles–mucin aggregates formed in different concentration of mucin. As shown in Figure 2A, significant

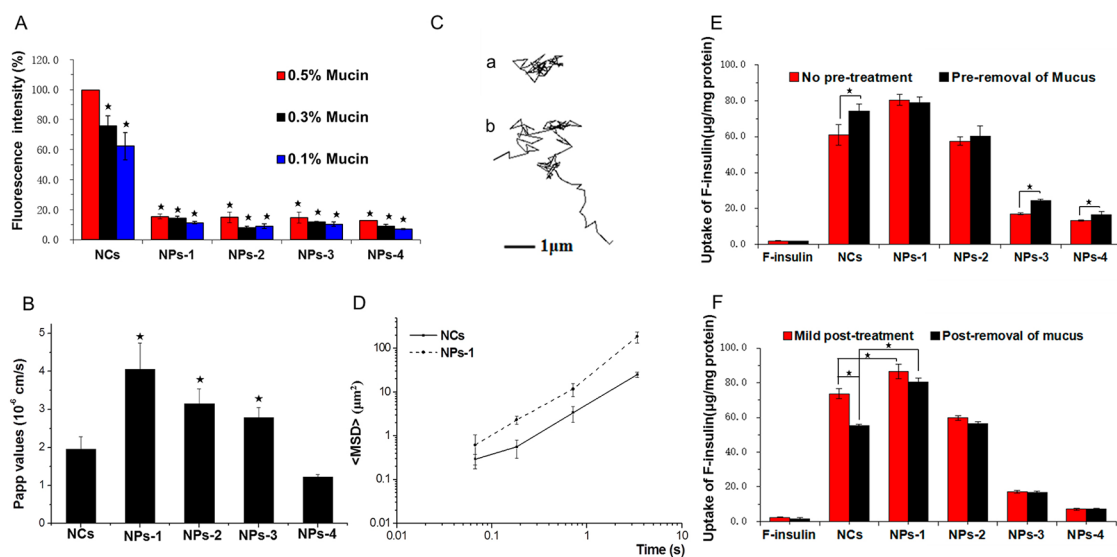


Figure 2. (A) The amount of particle–mucin aggregates formed at different concentration of mucin. The fluorescent intensity of aggregates for NCs at 0.5% mucin presented as control and normalized to 100%. Data are means \pm SD ($n = 3$), * $p < 0.05$, versus to control group. (B) Papp value of the particle permeation across mucus from donor and acceptor compartments of an Ussing Chamber System. Data are means \pm SD ($n = 3$), * $p < 0.05$, versus to NCs group. (C) Representative trajectories of the Brownian movement of NCs (a) and NPs-1 (b) in mucus at a time lapse of 4 s. (D) Ensemble-averaged geometric mean squared displacement ($\langle \text{MSD} \rangle$) as a function of time scale for NCs and NPs-1 in mucus. (E) Intracellular internalization of free F-insulin or particles on E12 cell with or without a pretreatment process to remove mucus. Data are means \pm SD ($n = 3$), * $p < 0.05$. (F) E12 cell associated F-insulin or particles after 2 h of incubation with different samples. After the incubation, the cells were treated with a mild wash to maximally preserve the mucus, or with a thorough washing process to remove the remained mucus. The amount of samples trapped in mucus was calculated as the difference between the groups of different post-treatment. Data are means \pm SD ($n = 3$), * $p < 0.05$.

lower amounts of aggregates were formed with all tested NPs compared with the insulin–CPP NCs. For example, at mucin concentration of 0.5% (w/v), the aggregates formed in NPs-1 groups were only 15.4% relative to those of NCs. However, no difference was observed among the four tested NPs. As all NPs with HPMA coating possessed hydrophilic surface with negative charge, both of the electrostatic and hydrophobic interaction between NPs and mucin can be avoided. Therefore, higher absolute value of the negative charge cannot further reduce the interaction. Then we tested the permeation of the NPs through the mucus layer using an Ussing Chamber System. Porcine intestinal mucus was amounted on a semipenetrating membrane, which separated the donor and acceptor compartments. The apparent permeability (Papp) values were calculated based on the accumulative amount of diffusion within 3 h (Figure 2B). Interestingly, although all NPs exhibited low affinity with mucin, the permeation ability decreased for NPs with higher absolute value of the surface charges. The NPs-1 exhibited the highest amount of permeation, which was 2-fold as that of NCs, whereas the permeation of NPs-4 was even lower than that of NCs. This phenomenon might be due to the electrostatic repulsion between the highly negatively charged NPs with the mucus, and correlated with those studies regarding MPP, in which electro-neutral surface was demonstrated as beneficial factor for mucus penetration.

To further investigate the behavior of the NCs and NPs in mucus, the motion of particles in mucus was analyzed using a multiple-particle tracking (MPT) method.²⁹ The trajectories of the particle motion were recorded (Supplementary Videos 1 and 2), and the examples of the motion trajectories in 4 s were shown in Figure 2C. The ensemble-averaged mean squared displacement ($\langle \text{MSD} \rangle$) for NCs and NPs-1 was calculated and shown in Figure 2D. The NC exhibited a highly constrained trajectory, whereas the trajectory of NPs-1 spanned much larger distances. At a time scale of 4 s, the ($\langle \text{MSD} \rangle$) of NPs-1 was 7.7-fold higher than that of Pen-ins NCs. The slope (α) of the logarithmic ($\langle \text{MSD} \rangle$) versus time scale plots was also calculated to reflect the extent of hindrance to diffusion.²⁹ Unobstructed Brownian diffusion is indicated by $\alpha = 1$, whereas $\alpha < 1$ suggests increasing impediment to diffusion as α approaches 0.³⁰ The average α of NPs-1 was 0.70, which is significantly larger than that of NCs (0.57). This result was consistent with the Brownian trajectories shown in Figure 2C and indicated a less hindered motion of NPs.

Cellular Internalization Study. For *in vitro* evaluation of the NPs, the HT29-MTX-E12 (E12) cell line was used in order to mimic the mucosa tissue,³¹ which consisted of the secreted mucus layer, as well as the absorptive epithelial cells. HT-29 is a human colorectal adenocarcinoma cell line with epithelial morphology with regard to the development of confluent monolayers and tight junction formation. E12 is a subclone isolated

from HT29 clone and characterized by high production of mucus, and thus an excellent model to study the nanoparticle behavior on mucosal tissue. All formulation exhibited no significant cytotoxicity on the E12 cells at the concentration from 50 to 250 $\mu\text{g/mL}$ as tested using MTT assay (Supporting Information Figure S9).

For the study of cellular internalization of NPs and the influence of mucus, a procedure was performed prior to the experiment to remove the secreted mucus layer using *N*-acetylcysteine (NAC).³² Then both pretreated and nontreated cells were incubated with different samples for 2 h, which was followed by a thorough washing process to remove the remained mucus and the attached samples.³² The amounts of internalized F-insulin were shown in Figure 2E. All tested formulations significantly increased the cellular internalization of F-insulin compared with free F-insulin solution. NPs-1 exhibited the highest uptake among all tested samples, which was ~20-fold higher compared with free insulin, despite the status of mucus. Notably, the uptake of NPs-1 was significantly higher compared with NCs when the mucus existed, while the two samples exhibited similar amounts of uptake with the preretreatment to remove mucus. Interestingly, for NPs-1 and NPs-2, there was no significant difference between the groups with and without the preremoval of mucus, while all other formulations exhibited less amount of uptake without the pretreatment. This result suggested that mucus layer acted as an obstacle for NCs, NPs-3 and NPs-4, but not for NPs-1 and NPs-2. We then investigated the amount of NPs that were likely to be trapped in the mucus layer in the uptake study. After the incubation, the cells were treated with a mild washing process to maximally preserve the mucus or a thorough washing process to remove the mucus. As shown in Figure 2F, higher amounts of F-insulin were associated with the cells with the mild post-treatment as compared to those with post-retreatment to remove mucus for the NCs. The amount of NCs stuck in mucus was estimated to be 24.8%. However, none of the NPs exhibited significant difference between the groups of different washing procedure. For NPs-3 and NPs-4, a very interesting phenomenon is that although the mucus inhibited the cellular uptake (Figure 2F), the amount of NPs trapped in the mucus was trivial (Figure 2E). This result correlated with the mucus permeation study and might be explained by the repulsion of the mucus against the NPs.

Structural Changes of NPs. As negatively charged hydrophilic material, the pHPMA that endow the NP with “mucus-inert” property may also inhibit the cellular uptake of the NP on the epithelial cells. Therefore, the CPP-rich nanocomplex core needs to be revealed in time when the NP contacts the epithelium. The coating of pHPMA on the surface of NCs was mediated by the electrostatic interaction between

the negatively charged MA-GG-OH segments on the polymer and the cationic CPP, and this noncovalent coating is dissociable over time. Therefore, we investigated the decoating process of NPs using FRET analysis. NPs prepared with fluorescent-labeled F-insulin and TRITC labeled HPMA polymers (T-pHPMA) exhibited strong FRET phenomenon in their intact form (Figure 1F). The dissociation of pHPMA from the NPs could be detected by observing the variation of the FRET intensity. As shown in Figure 3A,B, the fluorescence intensity of T-pHPMA decreased rapidly over time in mucus, while much smaller change was observed when the NPs were incubated in PBS. This phenomenon demonstrated that the pHPMA coating on the NPs was dissociable, and this process happened in a much faster rate in mucus than in PBS.

To further study the behavior and integrity of the NPs as they permeated through the mucus layer and the epithelium, the elevational distribution of different components of NPs on E12 cell monolayer was observed using confocal laser scanning microscopy (CLSM). As shown in Figure 3C, F-insulin and T-pHPMA were colocalized in the upper mucus layer at the apical side (0 μm in depth) as indicated by the overlapping of red and green signals, suggesting the NPs were in their intact form. Interestingly, less T-pHPMA was observed in deeper scanning, and there was very few colocalization from the depth of 30–60 μm . Green signals were observed in all layers from apical to basolateral side, indicating the efficient permeation of the drug through the mucus and the cell monolayer. Moreover, to study the integrity of the insulin-CPP nanocomplex core, cells were incubated with NPs prepared with F-insulin and TRITC-labeled penetratin (T-penetratin). CLSM images of E12 cells were taken and were shown in Figure 3D. A large proportion of the green and red signals were overlapped, which demonstrated that most of the insulin was still associated with the CPPs. These results implied that, as the NPs permeated through mucus, the pHPMA coating gradually dissociated from the CPP-rich nanocomplex core, while the latter remained intact and were internalized by the epithelium.

Transepithelial Transport and Intracellular Progression. Transport of F-insulin through E12 cell monolayer was evaluated using Transwell permeable supports. For each sample, the experiments were also performed with one group of cells pretreated with NAC to remove mucus. The apparent permeability coefficient (Papp) of F-insulin from apical to basolateral compartment through the cell monolayer was determined and shown in Figure 3E. All tested formulations exhibited higher Papp value compared with free insulin, which was consistent with the cellular internalized study. NPs-1 exhibited highest transepithelial transport for both pretreated and nontreated group, and was ~2.9 fold higher than that of free F-insulin. Similar to the cellular internalization study, the existence of mucus

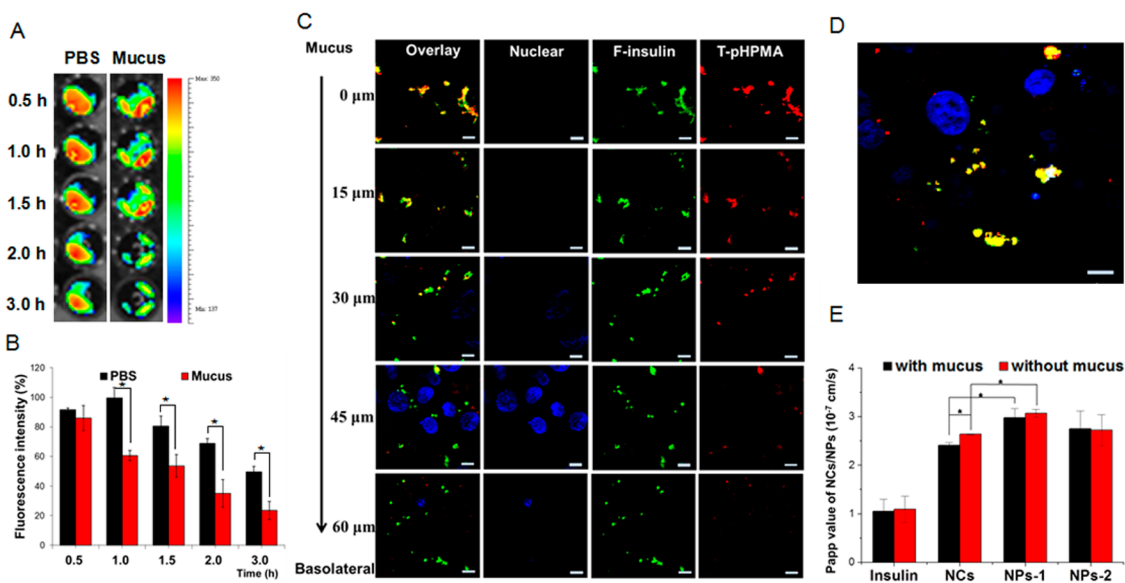


Figure 3. (A) FRET intensity of particles prepared with F-insulin and T-pHPMA after incubation in PBS or mucus for different times. The fluorescent intensity of TRITC represented the structural integrity of particles. (B) Quantitative analysis of FRET intensity for particles in PBS or mucus. Data was presented as the percentage of the intensity before incubation. Data are means \pm SD ($n = 3$), * $p < 0.05$. (C) CLSM images of the distribution of F-insulin and T-pHPMA in NPs on E12 cell monolayer from apical to basolateral side. Red, T-pHPMA; green, F-insulin; yellow, colocalization of F-insulin and T-pHPMA. Scale bars, 5 μ m. (D) CLSM images of E12 cells after incubation with NPs prepared with F-insulin and T-penetratin. Red, T-penetratin; green, F-insulin; yellow, colocalization of F-insulin and T-penetratin. Scale bars, 5 μ m. (E) Papp value of different samples across the E12 monolayer in the transepithelial transport study. Data are means \pm SD ($n = 3$), * $p < 0.05$.

has no significant influence on the transport of NPs-1 and NPs-2, while it reduced the transport of NCs. Besides, it was observed that the transepithelial electrical resistance (TEER) values of the cell monolayers were unchanged over time with the incubation of tested samples (Supporting Information, Figure S10), which indicated that the cell monolayer was intact and the translocation was only through a transcellular pathway.

Intracellular progression is a vital part of transcellular transport process. To investigate the intracellular trafficking of NCs and NPs, we first studied the localization of fluorescent labeled insulin in different organelles. The organelles, including endoplasmic reticulum (ER), Golgi apparatus, mitochondria and lysosome were stained using specific probes (red fluorescence). As shown in Figure 4A, colocalization of F-insulin with all of the four organelles was observed for both NCs and NPs. To better understand of the participation of the organelles in the particle progression, we then investigated the involvement of different organelles in the exocytosis of the particles. Previous reports demonstrated that ER and Golgi apparatus are vital components for secretory ER/Golgi pathway and endocytic recycling pathway.³³ Moreover, lysosomes also act as an important regulator for the exocytosis of internalized particles via fusion of the lysosomal membrane with plasma membrane.³⁴ Exocytosis of fluorescent-labeled particles on E12 cells was observed of all tested formulations (NCs, NPs-1 and NPs-2) as demonstrated in a chase-pulse study (Supporting Information

Figure S11). Furthermore, the exocytosis followed a time and energy dependent manner (Supporting Information Figures S12 and S13). We investigated the inhibition of exocytosis using specific progression inhibitors, including brefeldin A (ER/Golgi secretory pathway inhibitor), monensin (a Golgi/recycling endosome exocytosis pathway inhibitor), LY294002 and nocodazole (lysosomal exocytosis inhibitors). Incubation of the inhibitors with cells exhibited specific influence on the morphology of the corresponding organelles (Figure 4B). Both brefeldin A and monensin resulted in a remarkable inhibition of exocytosis of NCs or NPs (Figure 4C), suggesting the involvement of ER and Golgi apparatus in their intracellular trafficking. LY294002 and nocodazole also resulted in reduction their exocytosis (Figure 4D). These results indicated that ER, Golgi apparatus and lysosome were all involved in the intracellular trafficking of NCs and NPs. The pHPMA coating of the NPs did not affect the progression of the encapsulated drug relative to NCs.

In Vivo Hypoglycemic Effect and Pharmacokinetics. Finally, we evaluated the hypoglycemic effect and pharmacokinetics following oral administration of the NPs on diabetic rats. As shown in Figure 5A, similar to the saline, oral administration of free insulin solution failed to reduce the blood glucose level, while the administration of NPs-1 generated a remarkable hypoglycemic response with maximal 50% of blood glucose level reduction. The blood glucose level of the NPs-1 group was remained under 200 mg/dL for \sim 3 h, which is the

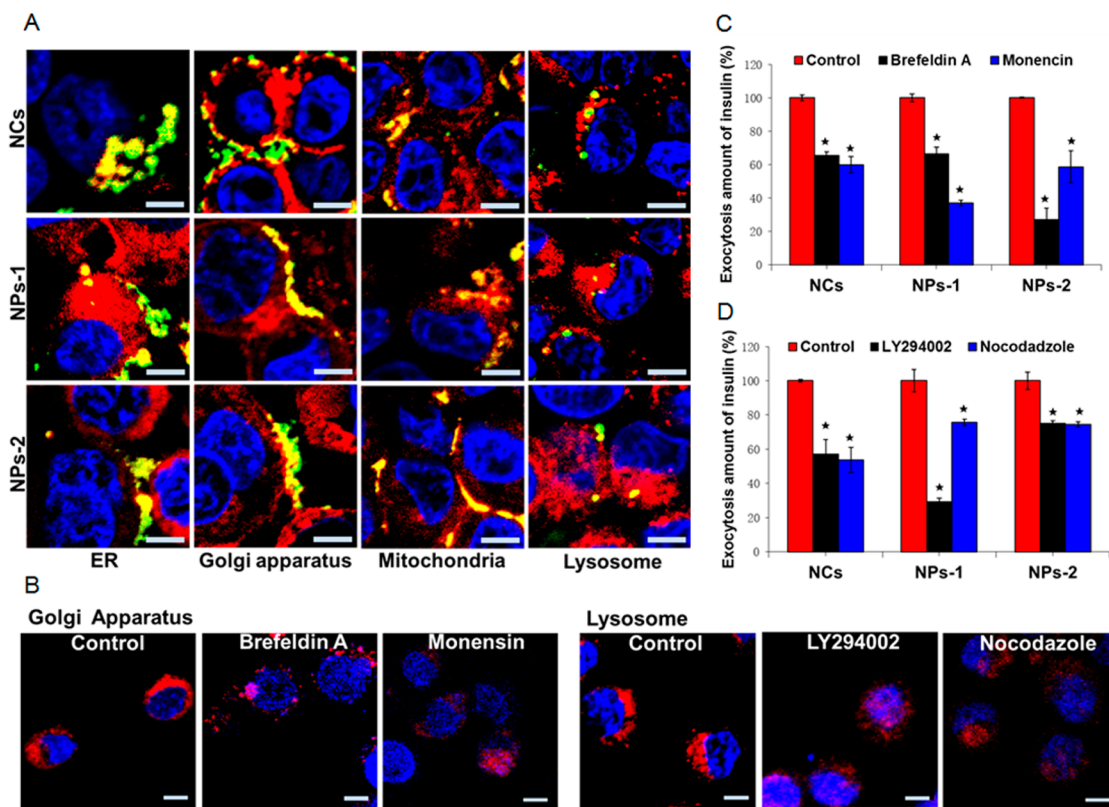


Figure 4. (A) CLSM images of E12 cells after incubation with different particles and specific organelle trackers. Green, F-insulin loaded NCs or NPs; red, specific organelle probes; blue, nuclear; yellow, colocalization green and red signals. Scale bars, 5 μ m. (B) CLSM images of Golgi apparatus and lysosome in E12 cells after the treatment with different specific organelles inhibitors. Golgi apparatus and lysosome were stained with specific probes (red) and the nucleus was stained with Dapi (blue). Scale bars, 5 μ m. (C) Influence of Golgi apparatus and ER inhibitors (brefeldin A and monensin) on the exocytosis of particles. Data was presented as the percentage of the exocytosis amount of the group without inhibitors. Data are means \pm SD ($n = 3$), * $p < 0.05$, versus control group. (D) Influence of lysosome inhibitors (LY294002 and nocodazole) on the exocytosis of particles. Data was presented as the percentage of the exocytosis amount of the group without inhibitors. Data are means \pm SD ($n = 3$), * $p < 0.05$, versus control group.

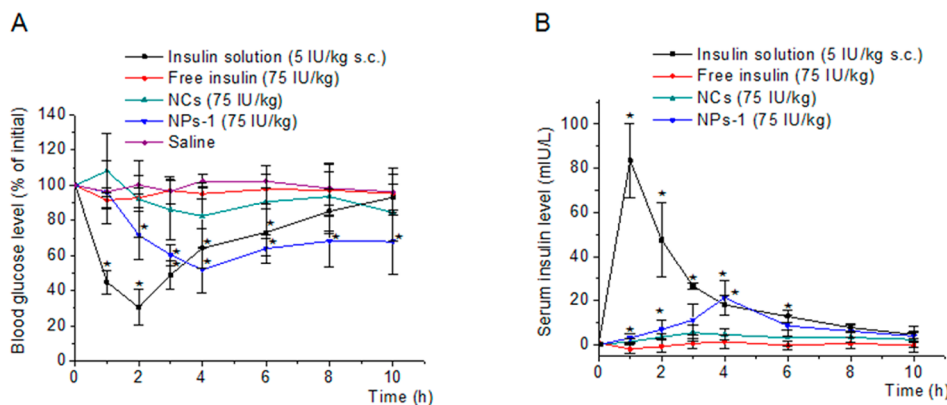


Figure 5. (A) Variation of blood glucose levels of diabetic rats after orally administering insulin loaded particles, insulin solution at dose of 75 IU/kg, subcutaneous injection with insulin solution at 5 IU/kg, or saline via gavage. Data are means \pm SD ($n = 5$), * $p < 0.05$ versus saline group. (B) Variation of serum insulin level of diabetic rats after orally administering insulin loaded particles or insulin solution at dose of 75 IU/kg, or subcutaneous injection with insulin solution at 5 IU/kg. Data are means \pm SD ($n = 5$), * $p < 0.05$ versus oral free insulin group.

threshold for the diagnosis of diabetes (Supporting Information Figure S14). In comparison, NCs only elicited a mild hypoglycemic response. The pharmacological availability (PA %) of different samples related to subcutaneous injection was shown in Table 2. NPs-1

demonstrated a PA % of 6.61%, which was 2.54-fold higher than that of NCs. The pharmacokinetic profiles of insulin were shown in Figure 5B. Subcutaneous injection of free insulin solution at 5 IU/kg resulted in a rapid increase in serum insulin concentration.

TABLE 2. Pharmacokinetic Parameters of Different Samples Following Administration^a

sample	dose (IU/kg)	AUC (mIU·h/L)	PA (%)	F (%)
Insulin s.c.	5	246.95 ± 20.06	-	100
Insulin oral	75	7.45 ± 6.66	1.38 ± 0.55	0.20 ± 0.18
NCs oral	75	53.59 ± 19.28	2.60 ± 0.60	1.45 ± 0.25
NPs-1 oral	75	111.19 ± 24.64	6.61 ± 0.62	3.02 ± 0.66

^aData are means ± SD ($n = 5$).

Orally administered NPs-1 generated a slower rise in serum insulin concentration, which reached the maximum concentration at 4 h. The pharmacokinetic parameters at the dose of 75 IU/kg were also shown in Table 2; NPs-1 exhibited a relative bioavailability of 3.02%, which is significantly higher than that of NCs (1.45%).

DISCUSSION AND CONCLUSIONS

The lack of nanocarriers with efficient mucus permeation and transepithelial absorption represents a significant barrier for safe and convenient oral applications of protein drugs in the treatment of chronic disease. One challenge in the oral nanocarrier development is that mucus permeation and epithelial absorption require different or even contradictory surface properties of the nanocarrier. The NP platform prepared herein was rationally designed to solve the dilemma in sequential mode, in which an expandable “mucus-inert” material was applied to disguise the NP as it permeated through the mucus, while the CPPs were subsequently revealed as transepithelial transport enhancers. To achieve optimal efficiency in both of these two processes, the NP was demonstrated to have several unique features.

One unique feature is that the hydrophilic coating is adjustable in charge density, which enables the screening of NP with a range of surface change. Surface property of particle is the most important factor that determines their diffusion in mucus.³⁵ In contrast with previously reported mucus penetrating NPs, which are generally covalently conjugated with PEG or coated with PEG containing surfactants,^{12,30} our distinctive NPs are assembled with a hydrophilic polymer that are amenable to different modifications. The pHPMAs synthesized with different ratios of MA-GG-OH monomer possessed a range of negative charges (Figure 1A, B). Therefore, the varied charge densities of the pHPMAs enabled not only a successful self-assembly of the material with the cationic NCs core as demonstrated by the FRET analysis (Figure 1F), but also the screening of the NP formulation to achieve the optimal surface property for mucus permeation (Figure 1E). Notably, all pHPMAs coated NPs possessed very low mucin affinity (Figure 2A), which suggested effectiveness of our “mucus-inert” strategy by concealing the cationic CPP-rich core under a high hydrophilic and

mildly negatively charged polymer. However, for the permeation across mucus, the NPs with relatively neutral surface (NPs-1 and NPs-2) exhibited better ability than those with higher negative charges (NPs-3 and NPs-4) (Figure 2B). This result is consistent with previous reports regarding the PEG-containing MPPs, and suggests that relative electroneutrality of NP surface is essential for efficient mucus permeation by avoiding both muco-adhesion and muco-repulsion.¹⁰ NPs-1 that showed excellent mucus permeation also demonstrated much less obstructed Brownian motion in mucus relative to the uncoated NCs (Figure 2C,D), and this phenomenon may largely increase the odds for the NPs to get access to the epithelial surface.

Another unique feature of the NP that enables its efficient absorption on epithelial tissue is the dissociation of pHPMAs from the NP surface in mucus, which simultaneously reveals the CPP-rich core, as shown in the schematic image of Figure 6. Neutral or negatively charged hydrophilic surface of NPs have been widely demonstrated to prevent the interaction of NPs with the cell membrane and thus inhibit their cellular uptake.¹⁶ For the developed NP platform, the pHPMAs that assembled on the particle surface gradually detached from cationic NC core during their permeation through the mucus (Figure 3A,B). Notably, this process happened in a much slower rate in saline solution than in mucus, which is a positive factor for the stability of the NPs and protection of encapsulated drugs in digestive intestinal fluid. Therefore, this technology avoids the drawback of low cell affinity of the traditional MPP. It is worth noting that, although pHPMAs dissociated from the NP as it was getting close to the epithelial cells, a large proportion of CPP–insulin nanocomplex core remained intact even after the internalization in the epithelial cells (Figure 3D). As expected, compared with the uncoated NCs, the coating of pHPMAs-1 (NPs-1) boosted the uptake of the particles on mucus covered epithelial cells (Figure 2E). However, reduced cell uptake was observed for NPs-3 and NPs-4 in comparison to the NCs (Figure 2E). This might be attributed to their lower surface charge that could reduce their affinity with cells, and might as well be the result of a slower dissociation rate of the pHPMAs-3, which possessed stronger interaction with the cationic NC core. Therefore, our study suggested the importance of the screening of the “mucus-inert” material with different charge density for an optimal overall performance.

Orally administered drug needs to be transported across the epithelium to be absorbed into systemic circulation. The insulin encapsulated in the CPP-rich nanocomplex was transported across the epithelial cell monolayer at a rate of 2.3-fold higher than of free drug (Figure 3E), and NPs-1 demonstrated even higher transport rate compared with the NCs. As we noted similar intracellular progression of NPs-1 and NCs

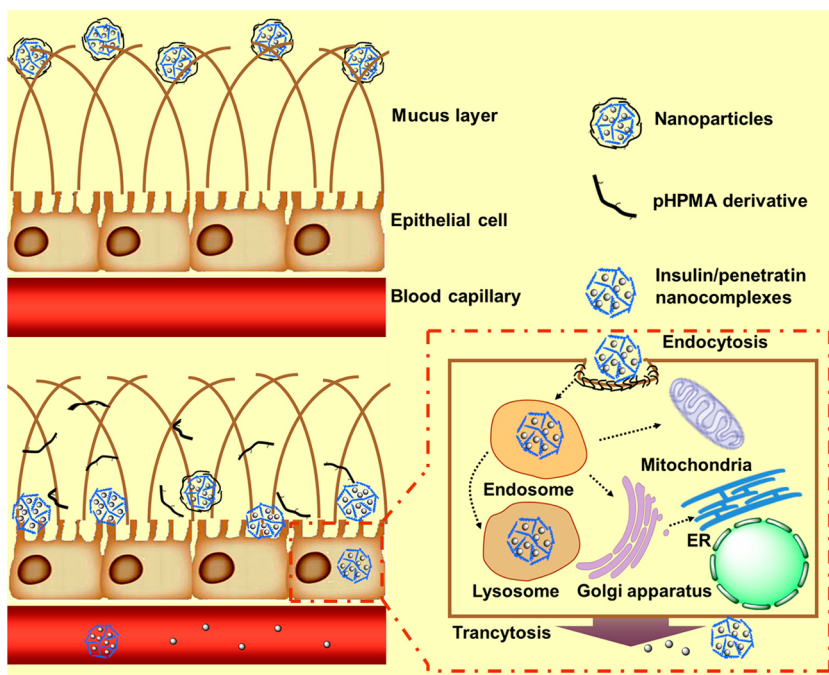


Figure 6. Schematic illustration of the process of the NP permeation across the mucus layer and the intracellular transport of NP in the epithelial cells.

(Figure 4A,C,D), which both involved secretory endoplasmic reticulum/Golgi pathway and endocytic recycling pathway, the improved transepithelial transport of NPs-1 may mainly be attributed to the better mucus permeation ability and timely revealing of the CPP-rich core for cell interaction. Moreover, the unchanged TEER value of cell monolayers throughout the treatment suggested that the translocation of drug happened through a transcellular pathway without compromising the integrity of the epithelium (Supporting Information Figure S10). Thus, this NP platform for transepithelial transport can avoid the potential safety issues associated with manipulating the permeability of epithelium.⁷ Furthermore, in diabetic rats, NPs-1 was able to generate an excellent hypoglycemic response and increase the serum insulin level after oral administration. The relative bioavailability of NPs-1 was 2.08-fold higher than that of NCs.

In summary, we rationally developed a distinctive self-assembled NP platform for effective oral delivery

of insulin. With systematic *in vitro* screening using mucus-secreting cells, NPs were demonstrated to possess the ability to overcome both the mucus barrier and epithelial barrier. We provide the first demonstration of enhanced mucus permeation of NP using pHPMA derivatives as a coating agent. However, an important fact that might need to be taken into account was that the mucus on the cell model might renew in a much slower rate than it happened in the gastrointestinal track. This might account for the higher difference between NP-1 and NC in the *in vivo* study compared with the *in vitro* results, and also suggested that further screening of the NP formulation using animal model might generate even better efficiency of delivery. In addition, this is the first example of applying dissociable hydrophilic coating and a cationic CPP-rich nanocomplex core to overcome both diffusion barrier of mucus and absorption barrier of epithelium, and our study might underscore the importance of overcoming the multiple barriers in a multistep strategy.

EXPERIMENTAL SECTION

Materials. Penetratin peptide was chemically synthesized by Kaijie Biopharmaceuticals Co., Ltd. (Sichuan, China). Porcine insulin (28.3 IU/mg) was purchased from Wanbang Bio-Chemical Co., Ltd. (Jiangsu, China). Fluorescein isothiocyanate (FITC), 3-(4,5-dimethyl-thiazol-2-yl)-2,5-diphenyl tetrazolium bromide (MTT), and nocodazole were all purchased from Sigma-Aldrich (St. Louis, MO). Lyso-Tracker Red and Mito-Tracker Red were purchased from Invitrogen (Carlsbad, CA). ER-Tracker Red, Golgi-Tracker Red, Brefeldin A, Monensin and LY294002 were acquired from Beyotime (Haimen, Jiangsu, China). Tetraethyl rhodamine isothiocyanate (TRITC) was purchased from FanboBiochemicals (Beijing, China). All chemical reagents utilized in study were analytic grade.

Synthesis and Characterization of pHPMA Derivatives. The monomers of *N*-(2-hydroxypropyl) methacrylamide (HPMA) and *N*-methacryloyl-glycylglycine (MA-GG-OH) were synthesized according to previous reports.^{36,37} Then three kinds of HPMA copolymer derivatives containing different amounts of MA-GG-OH monomers were synthesized by radical solution polymerization in absolute methanol (AIBN, 2 wt %; monomer concentration 12.5 wt %; molar ratio HPMA/MA-GG-OH were 95:5, 90:10, and 80:20, respectively). The copolymerization was performed in sealed ampules under nitrogen at 50 °C for 24 h. The pHMPA was isolated from polymerization mixture by precipitation into diethyl ether; then, dialyzed and lyophilized. The ¹H NMR spectra and mass spectrograms of monomers and

polymers were recorded on VANAN INOVA 400 and Agilent 6410 Triple Quad LC/MS, respectively. The molecular weight and polydispersity index (PDI) were determined by size exclusion chromatography on a Superose 200 10/300GL analytical column (Amersham Biosciences, NJ) using a Fast Protein Liquid Chromatography (AKTA FPLC) system (Amersham Biosciences, NJ). The charge density of pHMPA was estimated via acid–base titration and expressed as the millimole of carboxyl associated with 1 mg of pHMPA derivatives.

Preparation and Characterization of NPs. Insulin was dissolved in hydrochloric acid (HCl, 0.01M) at a concentration of 1.0 mg/mL (0.172 mM), and then the pH was adjusted to 7.0 using sodium hydroxide (NaOH, 1 M). Penetratin was dissolved in water at a concentration of 1.0 mg/mL (0.435 mM). The penetratin solution was added dropwise to insulin solution at a ratio of 1:2 (v/v) under stirring. The mixture was stirred at room temperature for 30 min, yielding an opalescent suspension (NCs). And then, NCs suspension was added dropwise to pHMPA derivatives' aqueous solution at an equal volume. The mixture was stirred for another 30 min, obtaining another opalescent suspension (NPs). Furthermore, fluorescent-labeled nanoparticles were prepared with the same method using FITC-labeled insulin (F-insulin). F-insulin was synthesized according to the previous reported procedure.³⁸

The nanoparticles were characterized for particle size and zeta potential with a Malvern Zetasizer NanoZS90 (Malvern Instruments Ltd., U.K.). The morphology of NCs/NPs was examined by transmission electron microscope (TEM, H-600, Hitachi, Japan). To evaluate the encapsulated efficiency (EE %) and drug loading efficiency (DL %), nanoparticle suspensions were centrifuged at 14 000 rpm for 20 min at 4 °C. After centrifugation, the amount of insulin in supernatant was measured by a reverse-phase high-performance liquid chromatography (RP-HPLC) method (Agilent 1200 series). In addition, the amount of free F-insulin in the supernatant of fluorescence-labeled nanoparticles was measured by Varioskan Flash Multimode Reader (Thermo Fisher Scientific). The excitation and emission wavelengths were set at 488 and 516 nm, respectively. To further investigate the interaction between insulin and pHMPA derivatives, FRET analysis was performed. Tetraethyl rhodamine isothiocyanate (TRITC) and fluorescein isothiocyanate (FITC) were used as FRET pairs. TRITC labeled F-insulin loaded nanoparticles were prepared using the procedure described above. The fluorescence intensity was measured through a fluorescence spectrophotometer (Shimadzu RF-5301, Japan) with an excitation wavelength of 440 nm and the emission spectrum was recorded from 500 to 600 nm. FRET efficiency (*E*) and the distance between the donor and acceptor (*R*) were calculated as following equations:

$$E = 1 - \frac{F_{DA}}{F_D}$$

$$R = R_0 - \sqrt{\frac{1}{E} - 1}$$

where F_{DA} is the intensity in the presence of the acceptor, F_D is the intensity in the absence of the acceptor, and R_0 is the Förster distance at 50% transfer efficiency. For FITC-TRITC, R_0 is 55 nm.²⁷

Mucus Permeation of NPs. For the measurement of particle–mucin aggregates, freshly NCs/NPs were dispersed in mucin solution of different concentration of 0.1%, 0.3%, 0.5% (m/v), vortexed and incubated for 30 min at 37 °C in a shaker. The mixture was centrifuged at 1500 rpm for 2 min and the precipitates were washed with PBS twice. Then, the precipitates were treated with 200 μL of NaOH (5 M); the mixtures were incubated for 10 min, and the fluorescence intensity was measured.

The permeation of NCs and NPs across mucus was measured using an Ussing chamber.³⁹ Briefly, 10 μL of mucus was placed uniformly in the oblong port which was covered with membrane filters (Merck Millipore, 2.0 μm). The donors were filled with 3 mL of Krebs-Ringer buffer containing test sample (F-insulin 0.05 mg/mL). The acceptors were filled with 3 mL of blank Krebs-Ringer buffer. The solutions on both sides were continuously aerated with gas (95% O₂ and 5% CO₂), and the device was maintained at 37 °C with a circulating water bath.

At the determined time points, an aliquot of sample (0.2 mL) was taken from the acceptors chamber and supplemented with equal volumes of blank Krebs-Ringer buffer. The amount of permeated F-insulin was determined via Varioskan Flash Multimode Reader (Thermo Fisher Scientific). The Papp was calculated using the following equation:

$$\text{Papp} = \frac{dQ}{dt} \times \frac{1}{A \times C_0}$$

where dQ/dt is the flux of F-insulin from donor side to acceptor side; C_0 is the initial concentration of insulin in the donor compartment, and A is the membrane area (cm²).

The Brownian movement of particles in mucus was investigated by MPT method.²⁹ The NCs/NPs dispersion was added to mucus sample, then transferred to microwells, and equilibrated for 30 min at 37 °C. Particles motion in the mucus was obtained using an inverted epifluorescence microscope (Nikon Ti-E, Japan). Movies were captured at 30 frames/s for 10 s, and were analyzed with NIS Elements 4.0 software to extract the *x* and *y* positional data over time. For each trajectory, the time-averaged mean squared displacement (MSD) was calculated as a function of time scale. The ensemble-averaged MSD ($\langle \text{MSD} \rangle$) for all particles in the mucus sample was calculated by taking the geometric mean of the individual particles' time-averaged MSDs.

Cell Culture. HT29-MTX-E12 (E12) cell were maintained in Dulbecco's Modified Eagle's Medium (DMEM; Invitrogen) with high glucose, 10% (v/v) fetal bovine serum (FBS; Sigma), 1% (v/v) nonessential amino acid, 1% (v/v) L-glutamine, and 1% penicillin and streptomycin (100 IU/mL). The cells were incubated at 37 °C in 5% CO₂. For the study of intracellular uptake, cytotoxicity, and uptake mechanism, E12 cells were seeded into 96-well plates (50 000 cells per well) and allowed to attach in growth medium at 37 °C in a 5% CO₂ incubator. For the establishment of *in vitro* cell monolayer, the E12 cells were seeded at a density of 10×10^4 cells/mL on a polycarbonate membrane (0.4 μm in pore size, diameter 6.5 mm, 0.33 cm² of cell growth area) in Costar Transwell 24 wells/plate (Corning Costar Corp.). Mediums in both upper and bottom compartments were changed every day. The transepithelial electrical resistance (TEER) was measured with an electrical resistance meter (Millicell ERS-2, Millipore) to monitor the integrity of cell monolayer.

Intracellular Uptake Studies. To investigate the cellular internalization of NPs and the influence of mucus, the mucus layer was removed a pretreatment process using NAC.³² Then, the pretreated and nontreated cells were incubated with test samples (F-insulin, 0.25 mg/mL) for 2 h, which was followed by a thorough washing process to remove the remained mucus and the attached samples. Then, cell lysis buffer was added, and the cell-associated fluorescence was measured (Varioskan Flash Multimode Reader, Thermo Fisher Scientific), and total protein was determined by BCA assay kit (KeyGen Biotech Co., Ltd., Nanjing, China). The uptake amounts of F-insulin were expressed as the quantity of F-insulin associated with 1 mg of cellular protein. To further evaluate the influence of mucus on the uptake of NCs/NPs, cells were incubated with test samples (F-insulin, 0.25 mg/mL) for 2 h. Then, cells were treated with a mild wash to maximally preserve the mucus, or with a thorough washing process to remove the remained mucus.³² Subsequently, the cell-associated fluorescence and the total protein were measured following the procedures described above.

Structural Changes of NPs. The integrity of NPs in mucus over time was investigated using FRET analysis. Briefly, the TRITC labeled HPMA derivative and FITC labeled insulin were used to prepare NPs. The NPs suspensions (at F-insulin concentration of 0.25 mg/mL) were loaded in a 96-well plate containing mucus or PBS (pH 7.4), and gently shaken in a thermostatic rotary shaker at 37 °C. At different time intervals, the plate was irradiated at a wavelength of 474 nm and imaged at an emission wavelength of 587 nm to obtain TRITC images.

To evaluate the structural changes of NPs in E12 cells, the TRITC labeled penetratin was synthesized,⁴⁰ and used to prepare the NPs. Then, cells were incubated with the NP for

1 h at 37 °C, and imaged using confocal laser scanning microscopy (FV1000, Olympus).

Transcellular Investigation. E12 cells were seeded on a polycarbonate membrane and cultured for 18–19 days. The cell monolayers with TEER values higher than 500 Ω·cm² were used for the experiment. Prior to the experiment, the media in the apical and basolateral chambers were replaced with pre-warmed Hanks balanced salt solution (HBSS) and the cells were equilibrated for 30 min at 37 °C. Then HBSS in apical chambers was replaced by 200 μL of fresh HBSS with test samples (F-insulin, 0.25 mg/mL). At certain time intervals, an aliquot of basolateral medium (200 μL) was withdrawn. The F-insulin concentration was determined and the Papp value was calculated accordingly. To investigate the influence of mucus on insulin permeation, experiments were also performed with a procedure to remove mucus with NAC.

Intracellular Trafficking. To study the intracellular trafficking of test NCs/NPs, the experiments were performed with organelle trackers or specific inhibitors as listed in Supporting Information Table S2.^{34,41} For colocalization analysis, E12 cells were first incubated with test samples (F-insulin, 0.25 mg/mL), for 1 h at 37 °C, and then the suspensions were replaced by fresh medium with different organelle trackers, including Lysotracker probe (50 nM), ER-Tracker probe (500 nM), Mito-Tracker probe (200 nM) and Golgi-Tracker (150 μg/mL). Then the cells were imaged using confocal microscope (FV1000, Olympus). In the inhibition study, cells were first incubated with different test samples (F-insulin, 0.25 mg/mL) for 2 h at 37 °C, and then washed with PBS twice. Subsequently, the cells were incubated with medium containing specific inhibitors for another 2 h. The amount of intracellular NCs/NPs was then measured as described above. The amount of NCs/NPs exocytosed out of the cells during incubation period was calculated.

Hypoglycemic Effect and Pharmacokinetic. The hypoglycemic effect and pharmacokinetic of the NPs following oral administration were evaluated on diabetic rats. All the experiments were approved by the Institutional Animal Care and Use Committee of Sichuan University. For the disease induction, male Sprague–Dawley rats weighting 180–220 g were injected with streptozotocin (65 mg/kg) as previously described.⁴² Blood glucose level was determined using a glucose meter (JPS-6, Yicheng Biotech. Co. Ltd. Beijing, China). The rat that exhibited fasting blood glucose level over 16.0 mM 1 week after treatment was considered to be diabetic. The rats were fasted overnight but allowed free access to water prior to the experiment. Rats ($n = 5$) were chosen per group such that the mean initial blood glucose levels were the same per group. Free insulin solution, NCs and NPs-1 were administrated at a dose of 75 IU/kg via gavage. Other groups of diabetic rats were subcutaneous injected (s.c.) with insulin solution at a dose of 5 IU/kg or oral administration with saline. Blood samples were collected from the tail veins prior to the administration and at different time intervals after the administration. Blood glucose level was determined using a glucose meter. Plasma insulin levels were quantified using porcine insulin ELISA kit (R&D System, Inc.), and the endogenous level of insulin (before administration) was subtracted from the tested value for each mouse. The area above the curve (AAC) of the blood glucose level and the area under the curve (AUC) of plasma insulin concentration curve were calculated. The pharmacological availability (PA %) and bioavailability (F %) relative to subcutaneous injection was analyzed as following equations:

$$PA(\%) = \frac{AAC_{\text{oral}} \times Dose_{\text{s.c.}}}{AAC_{\text{s.c.}} \times Dose_{\text{oral}}} \times 100$$

$$F(\%) = \frac{AUC_{\text{oral}} \times Dose_{\text{s.c.}}}{AUC_{\text{s.c.}} \times Dose_{\text{oral}}} \times 100$$

Statistics. Statistical analyses of the data were performed with SPSS program 16.0 by using two tail Student's *t* test. All experiments were performed in triplicate unless otherwise stated. Error bars used in this work are SD. A $p < 0.05$ is considered statistically significant (* $p < 0.05$).

Conflict of Interest: The authors declare no competing financial interest.

Acknowledgment. We gratefully acknowledge financial support from the National Natural Science Foundation of China (81173010).

Supporting Information Available: Characterizations of pHMPA derivatives, inhibitors with different functions used in the cellular exocytosis pathway study, spectra of monomers and polymer, insulin release profile, enzymatic degradation profiles of insulin with trypsin or α-chymotrypsin, cytotoxicity of NPs, TEER values of the cell monolayers over time with the incubation of tested samples, exocytosis of fluorescent-labeled NPs on E12 cells, blood glucose values and the videos of particle motion (avi). This material is available free of charge via the Internet at <http://pubs.acs.org>.

REFERENCES AND NOTES

1. Harris, J. M.; Chess, R. B. Effect of Pegylation on Pharmaceuticals. *Nat. Rev. Drug Discovery* **2003**, *2*, 214–221.
2. Chin, R. L.; Martinez, R.; Garmel, G. Gas Gangrene from Subcutaneous Insulin Administration. *Am. J. Emerg. Med.* **1993**, *11*, 622–625.
3. Carino, G. P.; Mathiowitz, E. Oral Insulin Delivery. *Adv. Drug Delivery Rev.* **1999**, *35*, 249–257.
4. Porter, C. J.; Trevaskis, N. L.; Charman, W. N. Lipids and Lipid-Based Formulations: Optimizing the Oral Delivery of Lipophilic Drugs. *Nat. Rev. Drug Discovery* **2007**, *6*, 231–248.
5. Mo, R.; Jiang, T.; Di, J.; Tai, W.; Gu, Z. Emerging Micro- and Nanotechnology Based Synthetic Approaches for Insulin Delivery. *Chem. Soc. Rev.* **2014**, *43*, 3595–3629.
6. Jin, Y.; Song, Y.; Zhu, X.; Zhou, D.; Chen, C.; Zhang, Z.; Huang, Y. Goblet Cell-Targeting Nanoparticles for Oral Insulin Delivery and the Influence of Mucus on Insulin Transport. *Biomaterials* **2012**, *33*, 1573–1582.
7. Pridgen, E. M.; Alexis, F.; Kuo, T. T.; Levy-Nissenbaum, E.; Karnik, R.; Blumberg, R. S.; Langer, R.; Farokhzad, O. C. Transepithelial Transport of Fc-Targeted Nanoparticles by the Neonatal Fc Receptor for Oral Delivery. *Sci. Transl. Med.* **2013**, *5*, 213ra167.
8. Ensign, L. M.; Cone, R.; Hanes, J. Oral Drug Delivery with Polymeric Nanoparticles: The Gastrointestinal Mucus Barriers. *Adv. Drug Delivery Rev.* **2012**, *64*, 557–570.
9. Dhuria, S. V.; Hanson, L. R.; Frey, W. H., II. Intranasal Delivery to the Central Nervous System: Mechanisms and Experimental Considerations. *J. Pharm. Sci.* **2010**, *99*, 1654–1673.
10. Lai, S. K.; Wang, Y. Y.; Hanes, J. Mucus-Penetrating Nanoparticles for Drug and Gene Delivery to Mucosal Tissues. *Adv. Drug Delivery Rev.* **2009**, *61*, 158–171.
11. Wang, Y. Y.; Lai, S. K.; Suk, J. S.; Pace, A.; Cone, R.; Hanes, J. Addressing the PEG Mucoadhesivity Paradox to Engineer Nanoparticles That "Slip" through the Human Mucus Barrier. *Angew. Chem., Int. Ed.* **2008**, *47*, 9726–9729.
12. Yang, M.; Lai, S. K.; Wang, Y. Y.; Zhong, W.; Happe, C.; Zhang, M.; Fu, J.; Hanes, J. Biodegradable Nanoparticles Composed Entirely of Safe Materials That Rapidly Penetrate Human Mucus. *Angew. Chem., Int. Ed.* **2011**, *50*, 2597–2600.
13. Xu, Q.; Boylan, N. J.; Cai, S.; Miao, B.; Patel, H.; Hanes, J. Scalable Method to Produce Biodegradable Nanoparticles That Rapidly Penetrate Human Mucus. *J. Controlled Release* **2013**, *170*, 279–286.
14. Yang, X. Z.; Du, J. Z.; Dou, S.; Mao, C. Q.; Long, H. Y.; Wang, J. Sheddable Ternary Nanoparticles for Tumor Acidity-Targeted siRNA Delivery. *ACS Nano* **2012**, *6*, 771–781.
15. Oh, E.; Delehanty, J. B.; Sapsford, K. E.; Susumu, K.; Goswami, R.; Blanco-Canosa, J. B.; Dawson, P. E.; Granek, J.; Shoff, M.; Zhang, Q.; et al. Cellular Uptake and Fate of PEGylated Gold Nanoparticles Is Dependent on Both Cell-Penetration Peptides and Particle Size. *ACS Nano* **2011**, *5*, 6434–6448.
16. Knop, K.; Hoogenboom, R.; Fischer, D.; Schubert, U. S. Poly(ethylene glycol) in Drug Delivery: Pros and Cons as Well as Potential Alternatives. *Angew. Chem., Int. Ed.* **2010**, *49*, 6288–6308.
17. Khafagy el, S.; Morishita, M. Oral Biodrug Delivery Using Cell-Penetrating Peptide. *Adv. Drug Delivery Rev.* **2012**, *64*, 531–539.

18. Khafagy el, S.; Morishita, M.; Isowa, K.; Imai, J.; Takayama, K. Effect of Cell-Penetrating Peptides on the Nasal Absorption of Insulin. *J. Controlled Release* **2009**, *133*, 103–108.
19. Zhu, X.; Shan, W.; Zhang, P.; Jin, Y.; Guan, S.; Fan, T.; Yang, Y.; Zhou, Z.; Huang, Y. Penetratin Derivative-Based Nanocomplexes for Enhanced Intestinal Insulin Delivery. *Mol. Pharmaceutics* **2014**, *11*, 317–328.
20. Madani, F.; Lindberg, S.; Langel, U.; Futaki, S.; Graslund, A. Mechanisms of Cellular Uptake of Cell-Penetrating Peptides. *J. Biophys.* **2011**, *2011*, 414729.
21. Duncan, R.; Vicent, M. J. Do HPMA Copolymer Conjugates Have a Future as Clinically Useful Nanomedicines? A Critical Overview of Current Status and Future Opportunities. *Adv. Drug Delivery Rev.* **2010**, *62*, 272–282.
22. Kopecek, J.; Kopeckova, P. HPMA Copolymers: Origins, Early Developments, Present, and Future. *Adv. Drug Delivery Rev.* **2010**, *62*, 122–149.
23. Ulbrich, K.; Subr, V. Structural and Chemical Aspects of HPMA Copolymers as Drug Carriers. *Adv. Drug Delivery Rev.* **2010**, *62*, 150–166.
24. Etrych, T.; Jelinkova, M.; Rihova, B.; Ulbrich, K. New HPMA Copolymers Containing Doxorubicin Bound via pH-Sensitive Linkage: Synthesis and Preliminary *in Vitro* and *in Vivo* Biological Properties. *J. Controlled Release* **2001**, *73*, 89–102.
25. Bissett, D.; Cassidy, J.; de Bono, J. S.; Muirhead, F.; Main, M.; Robson, L.; Fraier, D.; Magne, M. L.; Pellizzoni, C.; Porro, M. G.; et al. Phase I and Pharmacokinetic (PK) Study of MAG-CPT (PNU 166148): A Polymeric Derivative of Camptothecin (CPT). *Br. J. Cancer* **2004**, *91*, 50–55.
26. Seymour, L. W.; Ferry, D. R.; Kerr, D. J.; Rea, D.; Whitlock, M.; Poyner, R.; Boivin, C.; Hesslewood, S.; Twelves, C.; Blackie, R.; et al. Phase II Studies of Polymer-Doxorubicin (PK1, FCE28068) in the Treatment of Breast, Lung and Colorectal Cancer. *Int. J. Oncol.* **2009**, *34*, 1629–1636.
27. Lakowicz, J. R.; Masters, B. R. Principles of Fluorescence Spectroscopy. *J. Biomed. Opt.* **2008**, *13*, 9901.
28. Tang, B. C.; Dawson, M.; Lai, S. K.; Wang, Y. Y.; Suk, J. S.; Yang, M.; Zeitlin, P.; Boyle, M. P.; Fu, J.; Hanes, J. Biodegradable Polymer Nanoparticles That Rapidly Penetrate the Human Mucus Barrier. *Proc. Natl. Acad. Sci. U. S.A.* **2009**, *106*, 19268–19273.
29. Schuster, B. S.; Suk, J. S.; Woodworth, G. F.; Hanes, J. Nanoparticle Diffusion in Respiratory Mucus from Humans without Lung Disease. *Biomaterials* **2013**, *34*, 3439–3446.
30. Lai, S. K.; O'Hanlon, D. E.; Harrold, S.; Man, S. T.; Wang, Y. Y.; Cone, R.; Hanes, J. Rapid Transport of Large Polymeric Nanoparticles in Fresh Undiluted Human Mucus. *Proc. Natl. Acad. Sci. U.S.A.* **2007**, *104*, 1482–1487.
31. Behrens, I.; Stenberg, P.; Artursson, P.; Kissel, T. Transport of Lipophilic Drug Molecules in a New Mucus-Secreting Cell Culture Model Based on HT29-MTX Cells. *Pharm. Res.* **2001**, *18*, 1138–1145.
32. Behrens, I.; Pena, A. I.; Alonso, M. J.; Kissel, T. Comparative Uptake Studies of Bioadhesive and Non-Bioadhesive Nanoparticles in Human Intestinal Cell Lines and Rats: The Effect of Mucus on Particle Adsorption and Transport. *Pharm. Res.* **2002**, *19*, 1185–1193.
33. Burd, C. G. Physiology and Pathology of Endosome-to-Golgi Retrograde Sorting. *Traffic* **2011**, *12*, 948–955.
34. Yanes, R. E.; Tarn, D.; Hwang, A. A.; Ferris, D. P.; Sherman, S. P.; Thomas, C. R.; Lu, J.; Pyle, A. D.; Zink, J. I.; Tamanoi, F. Involvement of Lysosomal Exocytosis in the Excretion of Mesoporous Silica Nanoparticles and Enhancement of the Drug Delivery Effect by Exocytosis Inhibition. *Small* **2013**, *9*, 697–704.
35. Yang, M.; Lai, S. K.; Yu, T.; Wang, Y. Y.; Happe, C.; Zhong, W.; Zhang, M.; Anonuevo, A.; Fridley, C.; Hung, A.; et al. Nanoparticle Penetration of Human Cervicovaginal Mucus: The Effect of Polyvinyl Alcohol. *J. Controlled Release* **2014**, *192*, 202–208.
36. Ulbrich, K.; Subr, V.; Strohalm, J.; Plocova, D.; Jelinkova, M.; Rihova, B. Polymeric Drugs Based on Conjugates of Synthetic and Natural Macromolecules. I. Synthesis and Physico-Chemical Characterisation. *J. Controlled Release* **2000**, *64*, 63–79.
37. Duncan, R.; Cable, H. C.; Lloyd, J. B.; Rejmanová, P.; Kopeček, J. Polymers Containing Enzymatically Degradable Bonds, 7. Design of Oligopeptide Side-Chains in Poly[N-(2-hydroxypropyl)methacrylamide] Copolymers to Promote Efficient Degradation by Lysosomal Enzymes. *Macromol. Chem. Phys.* **1983**, *184*, 1997–2008.
38. Due, C.; Linnet, K.; Langeland Johansen, N.; Olsson, L. Analysis of Insulin Receptors on Heterogeneous Eukaryotic Cell Populations with Fluorochrome-Conjugated Insulin and Fluorescence-Activated Cell Sorter. Advantages and Limitations to the ¹²⁵I-Labelled Insulin Methodology. *Diabetologia* **1985**, *28*, 749–755.
39. Tanaka, S.; Podolsky, D. K.; Engel, E.; Guth, P. H.; Kaunitz, J. D. Human Spasmolytic Polypeptide Decreases Proton Permeation through Gastric Mucus *in Vivo* and *in Vitro*. *Am. J. Physiol.* **1997**, *272*, G1473–1480.
40. Bae, H. D.; Lee, K. On Employing a Translationally Controlled Tumor Protein-Derived Protein Transduction Domain Analog for Transmucosal Delivery of Drugs. *J. Controlled Release* **2013**, *170*, 358–364.
41. He, B.; Lin, P.; Jia, Z.; Du, W.; Qu, W.; Yuan, L.; Dai, W.; Zhang, H.; Wang, X.; Wang, J.; et al. The Transport Mechanisms of Polymer Nanoparticles in Caco-2 Epithelial Cells. *Biomaterials* **2013**, *34*, 6082–6098.
42. Sarmento, B.; Martins, S.; Ferreira, D.; Souto, E. B. Oral Insulin Delivery by Means of Solid Lipid Nanoparticles. *Int. J. Nanomed.* **2007**, *2*, 743–749.